SCIENTIFIC REPORTS

OPEN

Interface and material engineering for zigzag slab lasers

Fei Liu[1,2], Siyu Dong[1,2], Jinlong Zhang[1,2,3], Hongfei Jiao[1,2], Bin Ma[1,2], Zhanshan Wang[1,2,3] & Xinbin Cheng [1,2,3]

Laser damage of zigzag slab lasers occurs at interface between laser crystal and SiO_2 film. Although an additional HfO_2 layer could be used to manipulate electric-field on the crystal-film interface, their high absorption and polycrystalline structure were unacceptable. SiO_2 was then doped in HfO_2 to suppress its crystallization and to achieve low absorption by annealing. $Hf_xSi_{1-x}O_2$ nanocomposite layers were then inserted between laser crystal and SiO_2 film to minimize electric-field at crystal-film interface. Laser damage resistance of this new architecture is two times higher than that of traditional zigzag slab lasers.

The zigzag slab architecture is widely used in high power lasers. It can restrain thermally induced lensing and birefringence to obtain high output energy and exceptional beam quality[1–3]. Extremely high laser power has been obtained using zigzag slab laser architecture by Northrop Grumman[4,5]. Usually, the total internal reflection (TIR) in zigzag slab architecture is achieved by depositing lower index coatings on the surfaces of a laser crystal. Moreover, the coating is connected to the heat sink to take waste heat away[6]. When laser passes a zigzag path between two TIR surfaces in the crystal, strong electric-field intensity (EFI) is created. The coating must have low absorption, otherwise the joint effect of EFI and absorption will induce strong thermal effects and decrease the beam quality. SiO_2 is the dominant material for zigzag slab lasers due to its extremely low absorption from near ultraviolet to near infrared region.
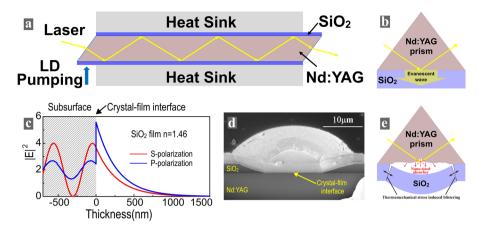
When the operating fluence of laser is higher and higher, the laser-induced damage becomes a severe issue. The crystal-film interface is the most vulnerable to laser damage, because massive nano-sized absorbers are created in vicinity of crystal-film interface due to surface contamination, polishing residues in the subsurface of the laser crystal, extraction of defects during coating deposition, or microstructure mismatch between the crystal and the film[7–10]. Laser damage at crystal-film interface is induced by the joint contribution of nano-sized absorbers and strong EFI[11–15]. The laser-induced damage threshold (LIDT) can be increased either by removing the massive nano-sized absorbers near crystal-film interface or by reducing EFI in vicinity of the crystal-film interface. Because it is quite challenging to remove all these nano-sized absorbers at crystal-film interface, the approach that reduces EFI is very promising. However, until now, the laser crystal with a SiO_2 coating is the only used configuration. No other slab laser architecture has been proposed to minimize EFI at crystal-film interface to improve LIDT. It is highly desirable to explore novel slab laser architecture to replace the traditional one.

Our previous studies have investigated the high reflection (HR) coatings that were irradiated from crystal-film interface[11,16]. It was found that adding a high index coating between the laser crystal and SiO_2 thin film could minimize the EFI at crystal-film interface and increase the laser damage resistance. However, there is a crucial difference between HR coatings and TIR coatings. Standing-wave EFI is created in HR coatings, whereas, evanescent-wave EFI develops in the SiO_2 layer for the TIR case. What a role that evanescent-wave EFI plays in laser damage and the experimental studies of interfacial damage of TIR surfaces have been rarely reported. In this work, the laser damage characteristics of traditional zigzag slab lasers was first investigated. Then, interface and material engineering were performed to find novel architecture of the zigzag slab lasers with increased LIDT.

Results and Discussion

Laser damage characteristics of the traditional zigzag slab lasers. The traditional configuration of the zigzag slab Nd:YAG laser working at 1064 nm is given in Fig. 1(a). The dimensions of slab are about 1.7 mm high, 67 mm long, 11 mm wide and 45° angle cut at the end. The crystalline orientation of Nd:YAG crystal is (111).

[1]MOE Key Laboratory of Advanced Micro-Structured Materials, Shanghai, 200092, China. [2]Institute of Precision Optical Engineering, School of Physics Science and Engineering, Tongji University, Shanghai, 200092, China. [3]IFSA Collaborative Innovation Center, Shanghai Jiao Tong University, Shanghai, 200240, China. Fei Liu and Siyu Dong contributed equally to this work. Correspondence and requests for materials should be addressed to X.C. (email: chengxb@tongji.edu.cn)

Figure 1. (**a**) Diagram of a zigzag slab laser. (**b**) Schematic, (**c**) EFI distributions, (**d**) damage morphology and (**e**) a phenomenological damage model of a Nd:YAG prism coated with a SiO$_2$ layer.

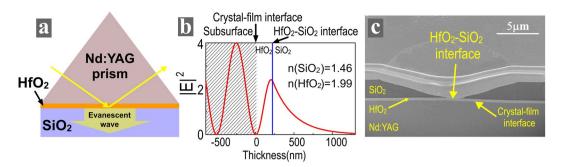| TIR configurations	Traditional TIR	TIR using HfO$_2$ layer	TIR using Hf$_x$Si$_{1-x}$O$_2$ layer
LIDT (J/cm^2, 1064 nm, 10 ns)	10 ± 2	6 ± 2	18 ± 2

Table 1. LIDTs of three TIR configurations.

The doping concentration of Nd:YAG crystal is about 0.05%. A 3 μm SiO$_2$ coating is deposited on the Nd:YAG crystal to achieve TIR and it is also connected to heat sink. The working laser passes a zigzag path between two TIR surfaces in the crystal and the pumping laser enters from the end of the crystal. It is difficult to directly study the laser damage characteristics of the zigzag slab lasers, therefore, an analog using Nd:YAG prisms coated with SiO$_2$ film was studied instead, as shown in Fig. 1(b). The Nd:YAG prisms with 0.05% doping and a size of 30 millimeters to a side were used for this study. The incident angle at crystal-film interface is set as 55° to achieve TIR.

The EFI distribution within the Nd:YAG crystal and SiO$_2$ thin film is given in Fig. 1(c). The standing-wave EFI is created in the subsurface of the crystal and the evanescent-wave EFI evolves in the SiO$_2$ coating. Because S-polarized EFI rather than P-polarized EFI could be reduced to zero at abrupt interfaces, only S-polarized laser damage is discussed here. The difference between S-polarized and P-polarized laser damage can be found in our previous work[16].

The LIDT testing was performed using 1064 nm, 10 ns pulses from a Nd:YAG laser having a TEM$_{00}$ mode. The raster scan method was used to obtain the LIDTs[17,18]. The LIDT of the traditional TIR configuration is about 10 ± 2 J/cm^2 (Table 1). The cross-sectional view of one representative damage morphology was revealed using a focus ion beam (FIB) technique, as shown in Fig. 1(d). It can be seen that the depth of the damage site is equal to the thickness of the SiO$_2$ coating, meaning that the laser damage initiated from the crystal-film interface. Both standing-wave EFI and evanescent-wave EFI are close to their maximum value at the crystal-film interface where nano-sized absorbers are concentrated, laser damage occurred preferentially at this interface, which reflects that evanescent-wave EFI at least plays a similar role in laser damage like standing-wave EFI. The formation of the damaged crater can be explained phenomenologically, as given in Fig. 1(e). The nano-sized absorbers at crystal-film interface is heated by the laser pulse to a very high temperature at which the defect-surrounding matrix is converted to the absorbing medium through photoionization by ultra violet (UV) radiation[19], thermionic emission of electrons[20] and the heat-transfer-induced band-gap collapse[21]. When the materials are heated to the melting temperature, thermomechanical damage occurs and results in blistering of the coating from Nd:YAG crystal.

Minimizing EFI at crystal-film interface using HfO$_2$ high index material. EFI in the traditional TIR configuration is fixed, additional approach must be found to engineer EFI at the crystal-film interface to improve LIDT. The HfO$_2$ film was explored to engineer the EFI at the crystal-film interface due to its optimal properties in the region from near ultraviolet to near infrared[22]. It was inserted between the Nd:YAG crystal and SiO$_2$ coating to minimize EFI at crystal-film interface, as shown in Fig. 2(a). By choosing thickness of the HfO$_2$ layer to be 230 nm, a destructive interference was created at the crystal-film interface and the EFI at this interface was decreased to zero, as given in Fig. 2(b). The side effects of adding a HfO$_2$ layer is that evanescent-wave EFI at the new HfO$_2$-SiO$_2$ interface is quite strong.

SiO$_2$ and HfO$_2$ coating on large optics is usually prepared using electron beam evaporation (EBE) process. However, the packing density of coatings prepared by EBE process is also low, and a lot of voids exist in the coatings, making their environmental stability and thermal conductivity poor. Here, the SiO$_2$ and HfO$_2$ coating was prepared using Ion assisted deposition (IAD) to achieve dense microstructure with good environmental stability and thermal conductivity. The absorption of SiO$_2$ coatings prepared by IAD process could be very low, however,

Figure 2. (**a**) Schematic, (**b**) EFI distribution and (**c**) damage morphology of a Nd:YAG prism coated with HfO_2 and SiO_2 films.
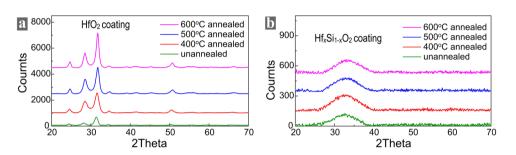

Figure 3. XRD curves of (**a**) HfO_2 and (**b**) $Hf_xSi_{1-x}O_2$ films annealed at different temperatures.

Films	SiO_2 unannealed	HfO_2 unannealed	HfO_2 annealed at 400 deg	HfO_2 annealed at 500 deg	HfO_2 annealed at 600 deg
Absorptivity (cm^{-1})	3.7×10^{-2}	3.1	7.0×10^{-1}	5.2×10^{-2}	4.5×10^{-2}

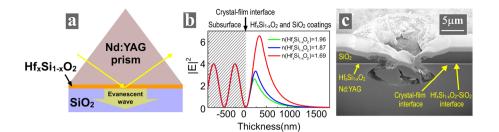**Table 2.** Absorptivity of SiO_2 film and HfO_2 film annealed at different temperatures.

HfO_2 coatings prepared by IAD process are always highly absorbing[23]. Its absorptivity was 2 orders higher than that of the SiO_2 coating, as given in Table 2.

The damage testing indicated that LIDT of this TIR configuration was only 6 ± 2 J/cm^2 (Table 1) and it is even worse than that of the traditional TIR configuration. The cross-sectional view of the representative damage morphology was examined to explain the LIDT result. Figure 2(c) shows that the laser damage initiated from the HfO_2-SiO_2 interface. The reason is that the highly absorbing HfO_2 coating leads to a concentration of intensive nano-sized absorbers at HfO_2-SiO_2 interface. Laser damage was created at this interface due to strong standing-wave EFI and evanescent-wave EFI here. The LIDT result reflects that the HfO_2-SiO_2 interface is even more vulnerable to the laser damage than the crystal-film interface.

Our previous study showed that, when the absorption of both coatings is very low, the HfO_2-SiO_2 interface is much more resistant to laser damage than the crystal-film interface[11]. So, annealing was attempted to reduce the absorption of the HfO_2 coating. The annealing temperature increases from 400 to 600 degrees centigrade with an increment step of 100 degrees centigrade. Table 2 shows that annealing at 600 degrees centigrade reduced the absorptivity of HfO_2 coatings by two orders and its absorption reaches to the level that is close to that of SiO_2 film. However, the cracking of the annealed HfO_2 film was identified using a Normarski microscope, as shown in Supplementary Figure S1. Previous studies reported that the crystalline states of HfO_2 films were changed during annealing, leading to volume change of the films, inducing strong associate stress and resulting in film cracking[22,24]. X-ray diffraction spectrometry (XRD) measurement revealed the change of the crystalline states during annealing, as given in Fig. 3(a). The XRD spectra shows that the HfO_2 films are polycrystalline and these films most contain the monoclinic phase of HfO_2 with preferred (111) orientation. The intensities of all the peaks become significantly higher when the annealing temperature increases. The large increase in peak intensity after high temperature annealing indicates that crystallite size has increased significantly. This leads to volume change of the films, induces strong associate stress and results in film cracking. As a result, annealing is not suitable to reduce the absorption of HfO_2 films.

Reducing EFI at crystal-film interface using $Hf_xSi_{1-x}O_2$ nanocomposite.

Two approaches have been proposed to suppress the crystallization of HfO_2 coatings during annealing. Nanolaminate is one approach that adds thin amorphous layers periodically into HfO_2 coatings to interrupt the crystallization[25]. However, this

Figure 4. (a) Schematic, (b) EFI distributions and (c) damage morphology of a Nd:YAG prism coated with $Hf_xSi_{1-x}O_2$ and SiO_2 films.

$Hf_xSi_{1-x}O_2$ Film	Unannealed	Annealed at 400 deg	Annealed at 500 deg	Annealed at 600 deg
Absorptivity (cm^{-1})	2.3	5.4×10^{-1}	4.5×10^{-2}	4.1×10^{-2}

Table 3. Absorptivity of $Hf_xSi_{1-x}O_2$ film annealed at different temperatures.

approach introduces many interfaces that will reduce the thermal conductivity and also reduce LIDT. It is not suitable to the current application. Nanocomposite is another approach that dopes amorphous material such as SiO_2 in HfO_2 to suppress crystallization[26–28]. It is possible to anneal $Hf_xSi_{1-x}O_2$ nanocomposite to reduce its absorption without changing its microstructure.

Here, $Hf_xSi_{1-x}O_2$ nanocomposite was prepared using a co-evaporation process with IAD. It was explored to engineer EFI at the crystal-film interface. The schematic of the configuration using $Hf_xSi_{1-x}O_2$ nanocomposite is given in Fig. 4(a). The refractive indices of the $Hf_xSi_{1-x}O_2$ nanocomposites can be varied in a wide range. Figure 4(b) presents the EFI distributions using $Hf_xSi_{1-x}O_2$ nanocomposites with three different refractive indices. Although zero EFI at crystal-film interface could be achieved by selecting proper thickness of each $Hf_xSi_{1-x}O_2$ nanocomposite layer, higher refractive index of the $Hf_xSi_{1-x}O_2$ nanocomposite results in lower EFI in the coatings. It is beneficial to use the highest refractive index of the $Hf_xSi_{1-x}O_2$ nanocomposite layer that does not crystalize at high annealing temperature. But the limitation is that the higher refractive index, the lower concentration of SiO_2 in $Hf_xSi_{1-x}O_2$ nanocomposite, and the worse resistant to crystallization at high annealing temperature. In our experiments, the refractive index of 1.87 at the wavelength of 1064 nm is the highest one that is still amorphous when the $Hf_xSi_{1-x}O_2$ nanocomposite layer was annealed at 600 degrees centigrade. When its layer thickness is 280 nm, the EFI at the crystal-film interface is zero.

The unannealed $Hf_xSi_{1-x}O_2$ nanocomposite layer was still highly absorbing. High temperature annealing effectively reduced its absorptivity to the level that is comparable to the SiO_2 layer, as given in Table 3. The XRD measurement of the $Hf_xSi_{1-x}O_2$ nanocomposite film annealed at different temperatures is given in Fig. 3(b). There are no sharp diffraction peaks in the XRD spectra of unannealed and annealed $Hf_xSi_{1-x}O_2$ films, which shows that the $Hf_xSi_{1-x}O_2$ films maintained amorphous microstructure during annealing.

The LIDT of this novel TIR configuration is 18 ± 2 J/cm^2 (Table 1), which is almost 2 times higher than that of the traditional TIR configuration (10 ± 2 J/cm^2). A cross-sectional view of the representative damage morphology of this TIR configuration is given in Fig. 4(c). The damage site has a larger and more irregular shape, and its depth is much deeper than the thickness of coatings. It can be seen that the laser damage initiated from a deep location within the subsurface of Nd:YAG crystal. EFI at the crystal-film interface is zero, laser damage would not start from here. Moreover, the absorption of the annealed $Hf_xSi_{1-x}O_2$ nanocomposite is very low, so the $Hf_xSi_{1-x}O_2$-SiO_2 interface has less nano-sized absorbers and is more resistant to laser damage compared to the crystal-film interface and the subsurface of the Nd:YAG crystal. It also reflects that the evanescent-wave EFI does not play a more detrimental role in laser damage than standing-wave EFI. As a result, only the nano-sized absorbers in the subsurface of the Nd:YAG crystal can trigger the laser-induced damage at the depth where peaks of EFI are located[11]. The absorptivity and density of nano-sized absorbers in the subsurface is much less than that at crystal-film interface, so the LIDT of this novel TIR configuration is almost 2 times higher than that of traditional one.

Conclusion

Interface and material engineering were performed to improve LIDT of zigzag slab lasers. A layer of high index material of HfO_2 was inserted between the Nd:YAG crystal and SiO_2 film to reduce the EFI at the crystal-film interface to be zero. However, the absorption of HfO_2 layer is too big and it was not practicable to reduce its absorption by annealing. $Hf_xSi_{1-x}O_2$ nanocomposite was then synthesized using co-evaporation process to solve this issue. $Hf_xSi_{1-x}O_2$ nanocomposite layer maintained its amorphous microstructure during annealing and achieved extremely low absorption. A novel configuration of zigzag slab lasers was proposed using $Hf_xSi_{1-x}O_2$ nanocomposite layer, whose LIDT was about two times higher than that of the traditional configuration of zigzag slab lasers.

Methods

Sample preparation. The Nd:YAG prisms were first carefully cleaned by ultrasonic cleaning process. The SiO_2 films and HfO_2 films were prepared using ion assisted deposition (IAD) process, and the $Hf_xSi_{1-x}O_2$ nano-composite films were prepared using co-evaporation process with IAD techniques. A schematic of co-evaporation process with IAD techniques is shown in Supplementary Figure S2. The $Hf_xSi_{1-x}O_2$ nanocomposite film was deposited on the substrates by co-evaporating HfO_2 and SiO_2 with IAD techniques. The two quartz crystal monitors were used to monitor the evaporation rates of two materials, and the two programmable masks were used to control the evaporation rates of two materials. The refractive indices of the $Hf_xSi_{1-x}O_2$ nanocomposites can be varied in a wide range with different relative evaporation rates of two materials. The details of the cleaning and deposition processes can be found in our previous papers[18,29,30]. Annealing processes of the films were performed in air at atmospheric pressure at 400, 500 and 600 °C for 3 hours.

Characterization methods. The LIDT testing was performed using 1.064 μm, 10 ns pulses from a Nd:YAG laser having a TEM 00 mode, a beam diameter of 1 mm and a repetition rate of 10 Hz. The raster scan method[17] was used to obtain the LIDTs. The laser fluence increased to the "damage fluence" with a 2 J/cm² increment. The damage morphologies may change during the raster scan test, so a single shot method was used to obtain representative damage morphologies. The damage morphologies were observed and characterized by an optical microscope, a scanning electron microscope (SEM) and a focus ion beam (FIB) equipment.

X-ray diffraction spectrometry (XRD) was used to characterize the crystallization of films with Cu Kα as the X-ray source. Data were collected in the θ–2θ (locked couple) mode from 2θ of 20–70° with a step size of 0.02°. Optical microscope was used to identify the cracking of the annealed HfO_2 coatings.

Photo-thermal technique was used to measure the absorptions of the films. The details of the absorption measurement can be found in our previous paper[23]. The absorptivity of coatings can be calculated by knowing the electric-field intensity (EFI) within them using the formula

$$A = \alpha \frac{n_1}{n_0} \int_0^l \frac{E^2(z)}{E_0^2} dz \tag{1}$$

where A is the absorption, α is the absorption coefficient, n_0 and n_1 are the refractive index of incident medium and film, E is the EFI and l is the thickness of the layer. The absorptivity of SiO_2 film and HfO_2 film prepared using electron beam evaporation (EBE) process and IAD process respectively is given in Supplementary Table S1.

References

1. Cha, Y. H. *et al.* Development and Characterization of a 400-W Slab-type Nd:YAG Gain Module. *Journal of the Optical Society of Korea* **16**, 53–56 (2012).
2. Matsumoto, O. *et al.* Analysis and Evaluation of Laser-Induced Damage of Zig-Zag Slab Laser Amplifier. *Japanese Journal of Applied Physics* **47**, 4531 (2008).
3. Palese, S. *et al.* High brightness, end-pumped, conduction cooled Nd:YAG zig-zag slab laser architecture. *Advanced Solid State Lasers, C. Marshall, ed* **50**, 41–46 (2001).
4. Goodno, G. D. *et al.* Coherent combination of high-power, zigzag slab lasers. *Opt. Lett.* **31**, 1247 (2006).
5. Mcnaught, S. J. *et al.* 100 kW coherently combined slab MOPAs. In Lasers and Electro-Optics, 2009 and 2009 Conference on Quantum electronics and Laser Science Conference. CLEO/QELS 2009. Conference on (pp. 1–2). IEEE (2009).
6. Aleknavičius, A. *et al.* Gain Measurements of Composite Nd: YAG Ceramic Slab Laser Active Element With Collinear Zigzag Pumping. In *Advanced Solid-State Photonics* (pp. AT4A–15). Optical Society of America (2012).
7. Rigatti, A. L. Cleaning process versus laser damage threshold of coated optical components. In *Optical Fabrication and Testing* (p. OMB3). Optical Society of America (2004).
8. Neauport, J., Lamaignere, L., Bercegol, H., Pilon, F. & Birolleau, J.-C. Polishing-induced contamination of fused silica optics and laser induced damage density at 351 nm. *Optics express* **13**, 10163–10171 (2005).
9. Lu, J., Cheng, X., Wang, Z., Liu, H. & Ji, Y. Separation of interface and volume absorption in Hf_O2 single layers. *Optical Engineering* **51**, 121814–121811–121814–121816 (2012).
10. Yu, Z. *et al.* Damage threshold influenced by the high absorption defect at the film–substrate interface under ultraviolet laser irradiation. *Optics letters* **38**, 4308–4311 (2013).
11. Cheng, X., Jiao, H., Lu, J., Ma, B. & Wang, Z. Nanosecond pulsed laser damage characteristics of HfO_2/SiO_2 high reflection coatings irradiated from crystal-film interface. *Optics express* **21**, 14867–14875 (2013).
12. Wang, Z. *et al.* Interfacial damage in a Ta_2O_5/SiO_2 double cavity filter irradiated by 1064 nm nanosecond laser pulses. *Optics express* **21**, 30623–30632 (2013).
13. Ye, X. *et al.* Advanced mitigation process (AMP) for improving laser damage threshold of fused silica optics. *Scientific reports* **6** (2016).
14. Chai, Y. *et al.* Laser-resistance sensitivity to substrate pit size of multilayer coatings. *Scientific reports* **6** (2016).
15. Tolenis, T. *et al.* Next generation highly resistant mirrors featuring all-silica layers. *Scientific reports* **7** (2017).
16. Cheng, X. *et al.* Optimal coating solution for a compact resonating cavity working at Brewster angle. *Optics express* **24**, 24313–24320 (2016).
17. Borden, M. R. *et al.* Improved method for laser damage testing coated optics. In *Laser-Induced Damage in Optical Materials: 2005* (Vol. 5991, p. 59912A). International Society for Optics and Photonics (2006).
18. Cheng, X. *et al.* The effect of an electric field on the thermomechanical damage of nodular defects in dielectric multilayer coatings irradiated by nanosecond laser pulses. *Light: Science and Applications* **2**, e80 (2013).
19. Koldunov, M. F., Manenkov, A. A. & Pocotilo, I. L. Theory of laser-induced damage to optical coatings: inclusion-initiated thermal explosion mechanism. In *Laser-Induced Damage in Optical Materials: 1993* (pp. 469–487). International Society for Optics and Photonics (1994).
20. Grua, P., Morreeuw, J., Bercegol, H., Jonusauskas, G. & Vallée, F. Electron kinetics and emission for metal nanoparticles exposed to intense laser pulses. *Physical Review B* **68**, 035424 (2003).
21. Wei, C., Shao, J., He, H., Yi, K. & Fan, Z. Mechanism initiated by nanoabsorber for UV nanosecond-pulse-driven damage of dielectric coatings. *Optics express* **16**, 3376–3382 (2008).
22. Park, J. W., Lee, D. K., Lim, D., Lee, H. & Choi, S. H. Optical properties of thermally annealed hafnium oxide and their correlation with structural change. *Journal of Applied Physics* **104**, 033521 (2008).

23. Ma, H. *et al*. Effect of boundary continuity on nanosecond laser damage of nodular defects in high-reflection coatings. *Optics Letters* **42**, 478–481 (2017).

24. Jena, S., Tokas, R. B., Rao, K. D., Thakur, S. & Sahoo, N. K. Annealing effects on microstructure and laser-induced damage threshold of HfO$_2$/SiO$_2$ multilayer mirrors. *Applied optics* **55**, 6108–6114 (2016).

25. Zhong, L., Daniel, W. L., Zhang, Z., Campbell, S. A. & Gladfelter, W. L. Atomic layer deposition, characterization, and dielectric properties of HfO$_2$/SiO$_2$ nanolaminates and comparisons with their homogeneous mixtures. *Chemical Vapor Deposition* **12**, 143–150 (2006).

26. Nguyen, N. V., Davydov, A. V., Chandler-Horowitz, D. & Frank, M. M. Sub-bandgap defect states in polycrystalline hafnium oxide and their suppression by admixture of silicon. *Applied Physics Letters* **87**, 192903 (2005).

27. Wang, T. & Ekerdt, J. G. Structure versus Thermal Stability: The Periodic Structure of Atomic Layer Deposition-Grown Al-Incorporated HfO$_2$ Films and Its Effects on Amorphous Stabilization. *Chemistry of Materials* **23**, 1679–1685 (2011).

28. Yurchuk, E. *et al*. Impact of layer thickness on the ferroelectric behaviour of silicon doped hafnium oxide thin films. *Thin Solid Films* **533**, 88–92 (2013).

29. Cheng, X. *et al*. Laser damage study of nodules in electron-beam-evaporated HfO$_2$/SiO$_2$ high reflectors. *Applied optics* **50**, C357–C363 (2011).

30. Shen, Z. *et al*. Influence of cleaning process on the laser-induced damage threshold of substrates. *Applied optics* **50**, C433–C440 (2011).

Acknowledgements

Author Contributions

X.C., F.L., S.D., and Z.W. conceived the experiment. S.D. and H.J. prepared the samples. F.L., J.Z. and B.M. performed EFI calculation, LIDT and XRD measurements and analyzed the data. F.L., S.D., and X.C. wrote the manuscript with contributions from Z.W. All authors discussed the results and commented on the manuscript. X.C. supervised the project.

Additional Information

Supplementary information accompanies this paper at https://doi.org/10.1038/s41598-017-16968-0.

Competing Interests: The authors declare that they have no competing interests.

Publisher's note: Springer Nature remains neutral with regard to jurisdictional claims in published maps and institutional affiliations.